

Synthesis and doping of organic-inorganic FAPbBr_3 perovskite nanostructures at room temperature

© D.A. Tatarinov¹, A.V. Baranov¹, A.N. Tsypkin², A.P. Litvin^{1,3}

¹ International research and educational center for physics of nanostructures, ITMO University, 197101 Saint-Petersburg, Russia

² Research and Educational Center for Photonics and Optoinformatics, ITMO University, 197101 Saint-Petersburg, Russia

³ College of Materials Science and Engineering, Jilin University, 130012 Changchun, China

e-mail: tatarinov@itmo.ru

Received March 22, 2024

Revised April 15, 2024

Accepted April 15, 2024

Synthesizing perovskite nanostructures at room temperature via ligand-assisted reprecipitation method allows precise control of their shape and size. Additionally, doping with specific ions enables the production of additional photoluminescence bands, thereby providing opportunities for tuning their optical properties. Methods for the synthesis of organic-inorganic perovskite nanostructures with different morphologies at room temperature are presented. By selecting the type and ratio of ligands, perovskite nanocrystals and nanoplates with the chemical formula FAPbBr_3 were synthesized. Postsynthetic treating pre-synthesized perovskite nanocrystals with the MnCl_2 precursor at room temperature enabled the production of $\text{Mn}^{2+}:\text{FAPbCl}_x\text{Br}_{3-x}$ nanocrystals with emission in two different spectral ranges.

Keywords: perovskite nanocrystals, perovskite nanoplates, doping, manganese dichloride, photoluminescence.

DOI: 10.61011/EOS.2024.04.58887.6179-24

1. Introduction

Lead halide perovskite nanostructures with different morphologies have been examined extensively in the last decade as candidate materials for devices requiring efficient and tunable radiation sources [1,2]. Perovskite nanocrystals (NCs) are characterized by high values of the light absorption cross section (multiphoton absorption included) and the photoluminescence quantum yield (PL QY), high stability of optical properties, and resistance to defects [3–5]. The synthesis of perovskite nanostructures with various morphologies (e.g., in the form of nanoplates (NPs)) allows one to obtain emission bands and exciton binding energies that are narrower and higher, respectively, than those in NCs. This is attributable to the quantum confinement effect and may be utilized in fabrication of efficient LEDs and lasers [6–8].

Organic-inorganic NCs and NPs with the perovskite structure (see Fig. 1, *a*) and chemical formula FAPbX_3 (FA is formamidinium; $X = \text{Cl}, \text{Br}, \text{I}$) are of great interest, since they may be synthesized at room temperature by reprecipitation in the presence of ligands (ligand-assisted reprecipitation, LARP) [9,10]. This method involves the preparation of a solution of precursors and ligands in a suitable polar solvent, which is then introduced into a non-polar antisolvent under vigorous stirring at room temperature. Adjusting the composition and proportions of ligands, one may control the morphology of synthesized perovskite

nanostructures accurately and efficiently to obtain NCs or NPs [3].

Alongside with adjustment of the morphology and chemical composition, doping is regarded in many research papers as a promising strategy for production of optoelectronic nanomaterials based on perovskite nanostructures with tailored optical properties [8,11]. Doping of perovskite nanostructures with certain types of ions is accompanied by the emergence of additional PL bands. For example, doping with manganese ions (Mn^{2+}) provides an opportunity to obtain an additional PL band in the red region of the spectrum [12–14]. Another important example is doping with lanthanides (specifically, ytterbium ions Yb^{3+}), which leads to the emergence of an additional PL band in the near infrared region of the spectrum [15,16]. The production of doped perovskite nanostructures normally requires synthesis at high temperatures, which makes it significantly more difficult to control the morphology of perovskite nanostructures. However, one may overcome this limitation by post-synthetic doping of pre-synthesized nanostructures with different morphologies [10,17]. The high adaptability and versatility of this approach in synthesis of doped perovskite NCs and NPs with specified optical properties was demonstrated in [18].

In the present study, methods for synthesis of organic-inorganic perovskite nanostructures with different morphologies are proposed, and a procedure of their doping with manganese ions via anion-cation exchange at room

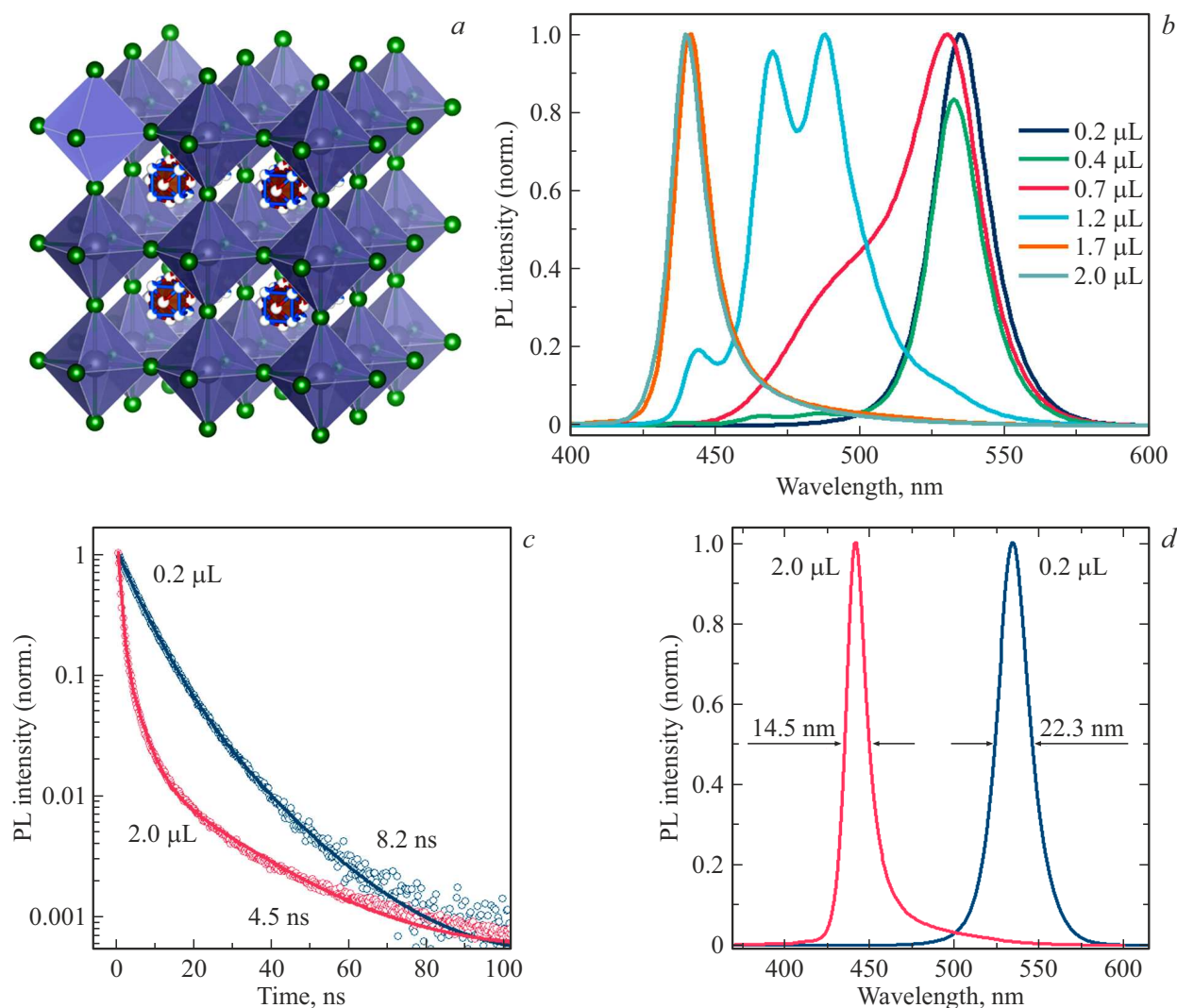


Figure 1. (a) Perovskite-type crystal structure with a chemical composition of FAPbBr_3 . Spectra (b, d) and decay curves (c) of PL for NCs and NPs of FAPbBr_3 synthesized with different amounts of OIAm.

temperature is detailed. Perovskite NCs and NPs with a chemical composition of FAPbBr_3 were obtained by varying the type and ratio of ligands. In addition, Mn^{2+} -doped $\text{FAPbCl}_x\text{Br}_{3-x}$ NCs with an additional emission band located at ~ 600 nm were produced using the MnCl_2 precursor with pre-synthesized perovskite NCs at room temperature.

2. Materials and research techniques

Organic-inorganic NCs and NPs with a perovskite structure and a chemical composition of FAPbBr_3 were produced by LARP. The following precursor solutions were prepared for this purpose: 0.1 mM PbBr_2 and 0.1 mM FABr in dimethylformamide (DMF). Following their thorough dissolution, 25 μL of the corresponding precursors were mixed, varying amounts of oleylamine (OIAm) were added, and the resulting solution was quickly introduced drop by drop

into 2 mL of toluene containing 40 μL of oleic acid (OA) under vigorous stirring. The amount of OIAm added varied with the 0.2–2 μL range.

The procedure of optimization of the synthesis of FAPbBr_3 NCs without side NP fractions was adapted from [9]. Specifically, a 0.1 mM solution (in 1 ml of DMF) of FABr and PbBr_2 precursors was prepared, and 200 μL of OA and 40 μL of OIAm were added to it. The obtained solution (100 μL) was introduced quickly into 3 mL of chloroform. NCs synthesized this way were purified by centrifugation with the addition of 1 mL of a 1 : 1 toluene/acetonitrile solution to 1 mL of the obtained NC solution. In order to synthesize FAPbBr_3 NPs, this method was modified by altering the type and ratio of solubilizers. Specifically, long-chain OA and OIAm were substituted with short-chain caproic acid and octylamine (OctAm) and used in different ratios.

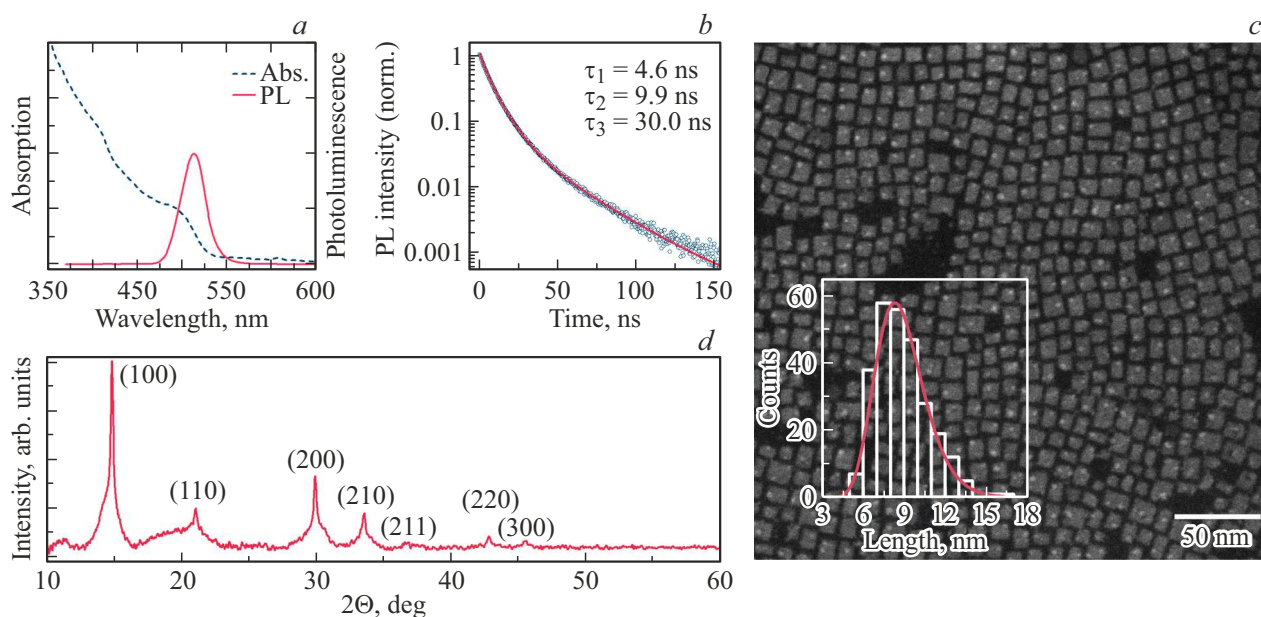


Figure 2. (a) Absorption and PL spectra, (b) PL decay curve, (c) TEM image (histogram of the NC size distribution is shown in the inset), and (d) X-ray diffraction pattern for FAPbBr₃ NCs.

The MnCl₂ precursor for post-synthetic doping of FAPbBr₃ NCs was prepared as follows: 0.1 mmol of anhydrous MnCl₂ and 15 μ L of OIAm were dissolved in 2 mL of toluene under stirring for 3 h at a temperature of 100°C and further 12 h of stirring at a temperature of 70°C. The indicated precursor amount was added to diluted FAPbBr₃ solutions. Following treatment, the NC solutions were centrifuged with the addition of an acetonitrile/toluene mixture (1 : 1) to remove excess MnCl₂. All post-synthetic processing procedures were performed in a glove box in an inert nitrogen atmosphere.

Absorption spectra were measured using a Shimadzu UV-3600 spectrophotometer. PL spectra were recorded with a Jasco FP-8200 spectrofluorimeter. A MicroTime 100 (PicoQuant) laser scanning luminescence microscope was used to study the PL decay kinetics. The decay of PL of Mn²⁺ ions was examined with a Cary Eclipse spectrofluorimeter. Microscopic images were obtained using a Zeiss Libra 200FE transmission electron microscope (TEM) at an accelerating voltage of 200 kV.

3. Results and discussion

Figure 1, *b* presents the PL spectra of the obtained colloidal solutions of FAPbBr₃ nanostructures. It is evident that the boundary amounts of added OIAm (0.2 and 2 μ L) correspond to the synthesis of pure samples (NCs and NPs, respectively), while mixtures of NPs of different thickness and NCs are obtained at intermediate values. The decay curves and PL spectra for FAPbBr₃ NCs and NPs and the weighted average PL decay times and FWHM values are shown in Figs. 1, *c* and *d*, respectively. Compared to NCs of

a similar chemical composition, NPs are characterized by a faster radiative relaxation and, consequently, shorter average PL decay times. Another distinctive feature is narrowing of the spectral line due to the quantum confinement effect in perovskite NPs, which is consistent with the FWHM reduction observed in the recorded spectra (from 22.3 nm for NCs to 14.5 nm for NPs).

The above-described synthesis process was optimized for fabrication of FAPbBr₃ NCs with the aim of producing stable colloidal solutions of NCs without side NP fractions. Chloroform was used as an antisolvent in this case, and the obtained NCs were then purified by centrifugation with the addition of a toluene/acetonitrile mixture. Figure 2, *a* shows the absorption and PL spectra of the obtained NCs; the PL decay curve is presented in Fig. 2, *b*), and the TEM image and X-ray diffraction pattern for this NC sample are shown in Figs. 2, *c*, *d*, respectively. No reaction by-products are observed for NCs synthesized with 0.2 μ L of OIAm, and the X-ray diffraction pattern makes it clear that this sample corresponds to the standard cubic phase of FAPbBr₃; the quantum yield of PL reaches 48% in this case. The average NC size is 8.7 ± 1.9 nm.

To obtain FAPbBr₃ NPs, this method was modified by introducing short-chain solubilizers (caproic acid and OctAm). Figures 3, *a–c* present the PL spectra corresponding to different combinations of amines/acids and their different ratios. It is worth noting that several reaction products (apparently, NPs of varying thickness and a certain amount of NCs) form when both oleic and caproic acid are used with an insufficient amount of OctAm. When the amine/acid ratio increases, predominant formation of a single NP fraction with a narrow PL spectrum is observed in both cases. Thus, a shift in acid-base equilibrium allows one to

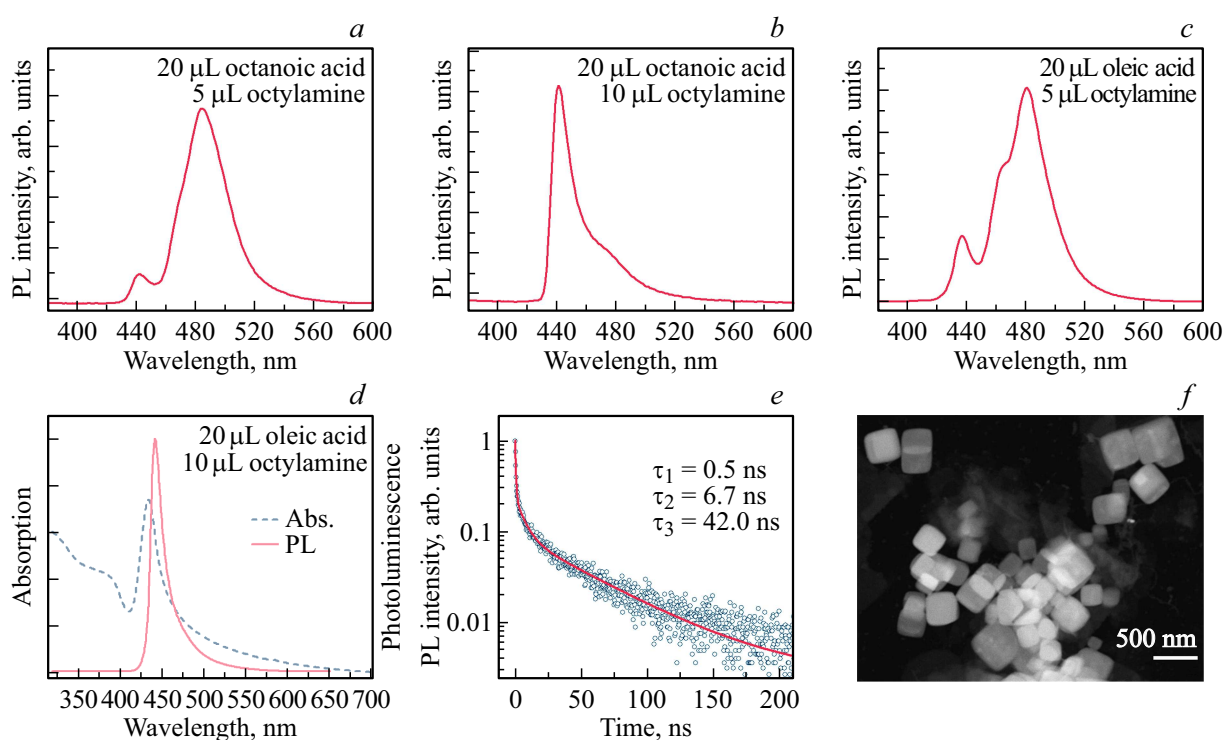


Figure 3. PL spectra (*a–c*) of FAPbBr_3 nanostructures obtained using oleic/caproic acids and octylamine in different ratios. Absorption and PL spectra (*d*), PL decay curve (*e*), and TEM image (*f*) for FAPbBr_3 NPs synthesized using 20 μL of oleic acid and 5 μL of octylamine.

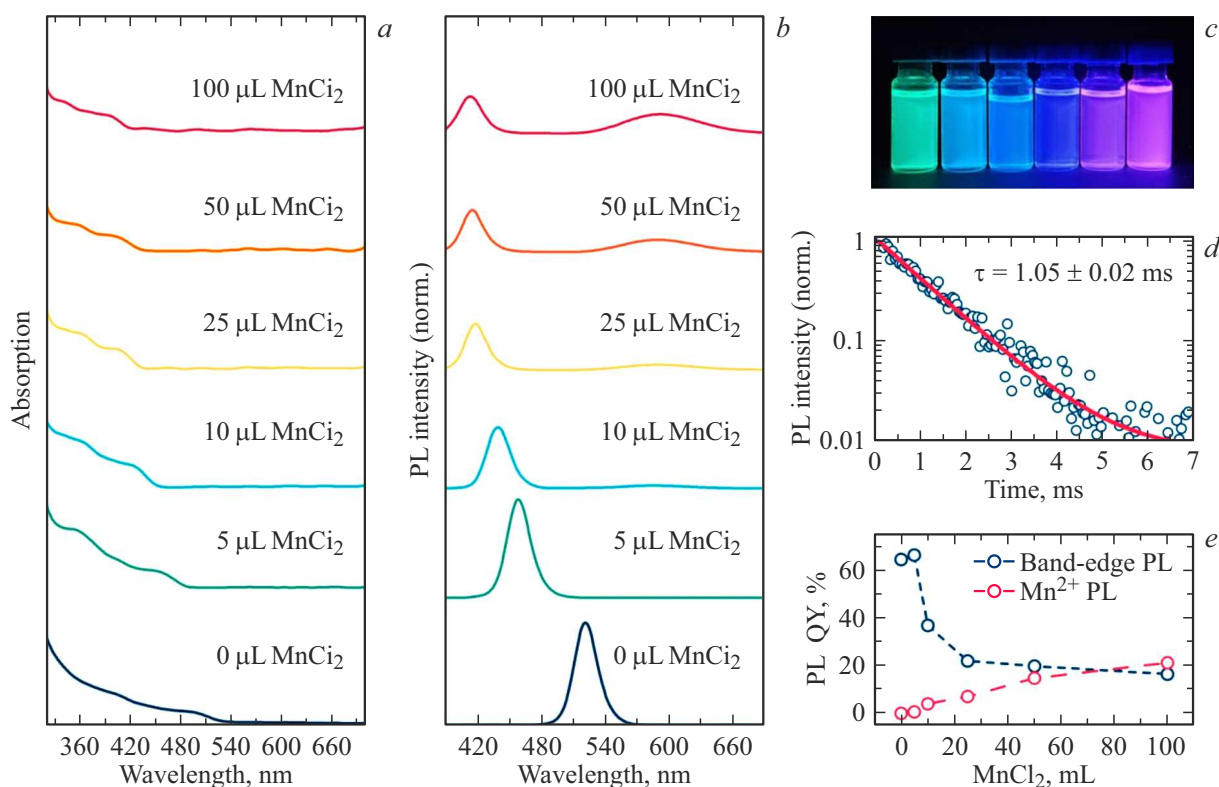


Figure 4. Absorption spectra (*a*), PL spectra (*b*), photographic image of samples under UV illumination (*c*), PL decay curve of Mn^{2+} ions (*d*), and PL QY values (*e*) for FAPbBr_3 NCs doped with Mn^{2+} ions with the use of different amounts of the MnCl_2 precursor.

control the morphology of synthesized structures in both examined approaches.

The best result was achieved with the use of OA and OctAm ligands mixed in a ratio of 20 μL of OA to 10 μL of OctAm. The PL and absorption spectra of the obtained NPs are shown in Fig. 3, *d*. The absorption and PL maxima are located at the wavelengths of 435 and 442 nm, respectively, which correspond to an NP thickness of 2 monolayers. According to literature data, this thickness is ~ 1.4 nm [9]. The quantum yield of PL was 25% in this case. The PL decay curve for FAPbBr₃ NPs may be approximated by a three-exponential function (see Fig. 3, *e*). The TEM image of the corresponding NPs presented in Fig. 3, *f* is indicative of a sufficiently high degree of homogeneity in their shape and size.

The developed method was extended to doping of perovskite nanostructures with other cations. To demonstrate this, FAPbBr₃ NCs were doped by introducing varying amounts of the MnCl₂ precursor. Figures 4, *a*, *b* show the absorption and PL spectra, respectively, for the original FAPbBr₃ NCs and NCs treated with different amounts of the MnCl₂ precursor. It can be seen that the gradual anion-cation exchange caused by the addition of a MnCl₂ solution leads to effective doping with Mn²⁺ ions that is accompanied by an enhancement of PL of Mn²⁺ ions and quenching of PL of the NC matrix. Figure 4, *c* presents the photographic image of colloidal solutions of Mn²⁺:FAPbCl_xBr_{3-x} NCs with different amounts of the MnCl₂ precursor (0–100 mL, left to right) under UV illumination. This image illustrates the changes in color of PL of samples, which are induced by the emergence of emission associated with Mn²⁺ ions. Specifically, doping with Mn²⁺ ions is manifested in the emergence of characteristic radiation centered at 600 nm. The PL decay curve of Mn²⁺ ions shown in Fig. 4, *d* may be approximated by a monoexponential function with a decay time of 1.05 ± 0.02 ms, which is typical of the forbidden ⁴T₁–⁶A₁ *d*–*d* transition [19,20]. The dependences of the PL quantum yield for the NC matrix and Mn²⁺ ions on the amount of added MnCl₂ are shown in Fig. 4, *e*. It can be seen that an increase in the amount of precursor added leads to gradual anion exchange and effective doping with Mn²⁺ ions. Thus, anion-cation doping, which is accompanied by an increase in the intensity of PL of Mn²⁺ ions and quenching of PL of the NC matrix, is observed. Specifically, the quantum yield of PL of Mn²⁺ ions reaches 20%, while the quantum yield of PL of the NC matrix decreases to 17% for the sample with 100 μL of MnCl₂ added.

4. Conclusion

Methods for synthesis of organic-inorganic perovskite nanostructures of various geometries with a chemical composition of FAPbBr₃ were developed, and their doping with Mn²⁺ ions was carried out at room temperature by means of anion-cation exchange. Perovskite NCs and NPs with

a composition of FAPbBr₃ were synthesized successfully by choosing carefully the types and ratios of ligands. In addition, the introduction of a precursor containing Mn²⁺ ions into a colloidal solution of pre-synthesized perovskite NCs allowed us to obtain FAPbCl_xBr_{3-x} NCs doped with Mn²⁺ ions with an additional emission band centered at a wavelength of 600 nm. These results expand the potential for tuning the optical properties of organic-inorganic perovskite nanostructures, opening up opportunities for their application in various kinds of optoelectronic devices.

Acknowledgments

The authors express their gratitude to the personnel of the Interdisciplinary Resource Centre for Nanotechnology (Research Park, St. Petersburg University) for the help with TEM imaging of samples, which was performed as part of project AAAA-A19-119091190094-6.

Funding

This study was supported by the Russian Science Foundation as part of scientific project No. 21-73-10131.

Conflict of interest

The authors declare that they have no conflict of interest.

References

- [1] J.S. Manser, J.A. Christians, P.V. Kamat. *Chem. Rev.*, **116** (21), 12956–13008 (2016). DOI: 10.1021/acs.chemrev.6b00136
- [2] Z. Cao, F. Hu, C. Zhang, S. Zhu, M. Xiao, X. Wang. *Adv. Photonics*, **2** (5), 8–10 (2020). DOI: 10.1117/1.AP.2.5.054001
- [3] A. Dey, J. Ye, A. De, E. Debroye, S.K. Ha, E. Bladt, A.S. Kshirsagar, Z. Wang, J. Yin, Y. Wang et al. *ACS Nano.*, **15** (7), 10775–10981 (2021). DOI: 10.1021/acsnano.0c08903
- [4] M. Liu, G.K. Grandhi, S. Matta, K. Mokurla, A. Litvin, S. Russo, P. Vivo. *Adv. Photonics Res.*, **2** (3), 2000118 (2021). DOI: 10.1002/adpr.202000118
- [5] Y. Li, X. Zhang, H. Huang, S.V. Kershaw, A.L. Rogach. *Mater. Today*, **32**, 204–221 (2020). DOI: 10.1016/j.mattod.2019.06.007
- [6] P. Tyagi, S.M. Arveson, W.A. Tisdale. *J. Phys. Chem. Lett.*, **6** (10), 1911–1916 (2015). DOI: 10.1021/ACS.JPCLETT.5B00664/SUPPL_FILE/JZ5B00664.SL001.PDF
- [7] Y. Bekenstein, B.A. Koscher, S.W. Eaton, P. Yang, A.P. Alivisatos. *J. Am. Chem. Soc.*, **137** (51), 16008–16011 (2015). DOI: 10.1021/jacs.5b11199
- [8] A.P. Litvin, I.V. Margaryan, W. Yin, X. Zhang, W. Zheng, A.L. Rogach. *Adv. Opt. Mater.*, (2023). DOI: 10.1002/adom.202301001
- [9] I. Levchuk, A. Osvet, X. Tang, M. Brandl, J.D. Perea, F. Hoegl, G.J. Matt, R. Hock, M. Batentschuk, C.J. Brabec. *Nano Lett.*, **17** (5), 2765–2770 (2017). DOI: 10.1021/acs.nanolett.6b04781

- [10] D.A. Tatarinov, A.V. Sokolova, I.D. Skurlov, D.V. Danilov, A.V. Koroleva, N.K. Kuzmenko, Y.A. Timkina, M.A. Baranov, E.V. Zhizhin, A.N. Tsyarkin et al. *J. Mater. Chem. C*, **11**, 5657–5666 (2023). DOI: 10.1039/D3TC00180F
- [11] S. Kachhap, S. Singh, A.K. Singh, S.K. Singh. *J. Mater. Chem. C*, **10** (10), 3647–3676 (2022). DOI: 10.1039/D1TC05506B
- [12] W. Liu, Q. Lin, H. Li, K. Wu, I. Robel, J.M. Pietryga, V.I. Klimov. *J. Am. Chem. Soc.*, **138** (45), 14954–14961 (2016). DOI: 10.1021/jacs.6b08085
- [13] M.C. De Siena, D.E. Sommer, S.E. Creutz, S.T. Dunham, D.R. Gamelin. *Chem. Mater.*, **31** (18), 7711–7722 (2019). DOI: 10.1021/acs.chemmater.9b02646
- [14] C. Zhao, J. Shi, H. Huang, Q. Zhao, X. Zhang, J. Yuan. *Small Sci.*, **4** (1), (2024). DOI: 10.1002/smssc.202300132
- [15] N.V. Tepliakov, A.V. Sokolova, D.A. Tatarinov, X.Zhang, W. Zheng, A.P. Litvin, A.L. Rogach. *Nano Lett.*, **24** (11), 3347–3354 (2024). DOI: 10.1021/acs.nanolett.3c04881
- [16] N. Ding, W. Xu, D. Zhou, Y. Ji, Y. Wang, R. Sun, X. Bai, J. Zhou, H. Song. *Nano Energy.*, **78** 105278 (2020). DOI: 10.1016/j.nanoen.2020.105278
- [17] T. Qiao, D. Parobek, Y. Dong, E. Ha, D.H. Son. *Nanoscale*, **11** (12), 5247–5253 (2019). DOI: 10.1039/C8NR10439E
- [18] S. Huang, B. Wang, Q. Zhang, Z. Li, A. Shan, L. Li. *Adv. Opt. Mater.*, **6** (6), 1701106 (2018). DOI: 10.1002/adom.201701106
- [19] X. Yuan, S. Ji, M.C. De Siena, L. Fei, Z. Zhao, Y. Wang, H. Li, J. Zhao, D.R. Gamelin. *Chem. Mater.*, **29** (18), 8003–8011 (2017). DOI: 10.1021/acs.chemmater.7b03311
- [20] D. Chen, G. Fang, X. Chen. *ACS Appl. Mater. Interfaces*, **9** (46), 40477–40487 (2017). DOI: 10.1021/acsami.7b14471

Translated by D.Safin